Measurement System to Determine the Seebeck Coefficient and Electrical Conductivity of Thin Films

Gustavo G. Dalkiranis, João H. C. Bocchi, Bruno Bassi Millan Torres, Aitor F. Lopeandia, Osvaldo N. Oliveira Jr., and Gregório C. Faria

***Abstract*— Thermoelectric (TE) materials are promising for energy-generating devices, and their design depends on a fast, precise determination of their Seebeck coefficient and electrical conductivity. Herein, a low-cost setup was developed to determine the Seebeck coefficient and electrical conductivity of thin films, allowing the calculation of the power factor (PF) (PF = $S^2\sigma$). The system was validated by measuring the Seebeck coefficient and electrical conductivity of poly(3,4-ethylenedioxythiophene) polystyrene sulfonate (PEDOT:PSS), a widely used material in organic electronics and TE generators. The results demonstrate the high resolution of our system, with obtained values of 0.1 μV/K for Seebeck coefficient, 0.1 S/cm for electrical conductivity, and 0.1 μW/K^2 for PF. A detailed description of the fabrication of the measurement setup is provided, with the aim of making thermoelectricity accessible to any research laboratory, even in places with limited budgets.**

***Index Terms*— Electrical conductivity, instrumentation, measurement system, power factor (PF), Seebeck coefficient, thermoelectricity.**

I. Introduction

THERMOELECTRIC (TE) energy generation is promising to address energy demands, especially for portable devices and low-power consumer electronics [1], [2], [3]. It may exploit the temperature difference existing in almost all mechanical and electrical systems, as in a car (engine/car body), and in a solar panel (face exposed to the sun/face unexposed) to name a few [4]. In fact, of all the energy produced worldwide, only 40% is used to perform actual work, the remainder being lost as waste heat [5], [6]. In this context, TE materials can play a significant role converting thermal energy into electricity. Indeed, by applying a temperature gradient to a TE material, a heat flow is established between the electrodes of the device, resulting in the diffusion of charge carriers from the hotter to the colder region. This phenomenon is known as the Seebeck Effect, first described in 1821 by Thomas Johann Seebeck [7], [8], [9], [10]. TE generators can not only be used to recover heat waste, but also to convert the heat radiated by the sun into electricity, complementing photovoltaic devices as infrared (IR) harvesters or operating as independent systems. They are often used in conditions of intense light and heat, and are then referred to as solar TE generators (STEGs) [11]. In addition, geothermal energy, which harvest heat from the Earth's interior, is one of the largest renewable sources available. It is characterized by its independence from weather conditions, providing stability and offering high energy source potential. This source can be utilized for power generation through TE devices, which exploits the temperature difference between the subsurface and the surface as a heat source [12].

An important parameter of TE materials is the figure of merit (denoted as "ZT"), which considers the relationship between the Seebeck coefficient (S), thermal (k) and electrical (σ) conductivities according to (1) [8], [9], [10], [13]

$$ZT = \frac{S^2\sigma}{k}T \tag{1}$$

where T is the average temperature between the cold and hot sources. Generally, materials with figure of merit (ZT) higher than 1 at room temperature are desirable for TE generators. It is important to note that while ZT is a key indicator of a TE material's performance as a generator, different ZT may be more relevant when the material is used for sensing applications. Therefore, the material must have low thermal conductivity and a high power factor (PF) (PF = $S^2\sigma$) [8], [9], [10], [13]. By increasing the Seebeck coefficient of the material and/or the electrical conductivity, an increase in the PF is obtained. It is important to highlight that it is challenging to manipulate only a single parameter of the figure of merit, since the Seebeck coefficient, electrical and thermal conductivity are intrinsically interdependent [14], [15].

To determine the Seebeck coefficient, as defined in (2) [8], [9], [10], [13], one needs to measure the temperature difference applied to the borders of a material accurately, in addition to

Received 14 October 2024; revised 17 January 2025; accepted 2 March 2025. Date of publication 20 March 2025; date of current version 8 April 2025. This work was supported in part by the National Institute of Science and Technology for Organic Electronics (INCT/INEO), in part by the National Council for Scientific and Technological Development (CNPq, Brazil) under Grant 141507/2023-3, in part by São Paulo Research Foundation (FAPESP, Brazil) under Grant 2018/22214-6 and Grant 2019/26375-7, and in part by the Coordination of Superior Level Staff Improvement (CAPES, Brazil). The Associate Editor coordinating the review process was Dr. Jorge Alfredo Ardila-Rey. *(Gustavo G. Dalkiranis and João H. C. Bocchi contributed equally to this work.) (Corresponding author: Gustavo G. Dalkiranis.)*

Gustavo G. Dalkiranis, João H. C. Bocchi, Bruno Bassi Millan Torres, Osvaldo N. Oliveira Jr., and Gregório C. Faria are with Sao Carlos Institute of Physics, University of Sao Paulo, São Carlos, São Paulo 13560-970, Brazil (e-mail: dalkiranis@gmail.com).

Aitor F. Lopeandia is with the Departament de Física, Universitat Autònoma de Barcelona, 08193 Cerdanyola del Vallès, Spain, and also with the Catalan Institute of Nanoscience and Nanotechnology (ICN2), CSIC and BIST, 08193 Barcelona, Spain.

This article has supplementary downloadable material available at https://doi.org/10.1109/TIM.2025.3553254, provided by the authors.

Digital Object Identifier 10.1109/TIM.2025.3553254

the voltage difference generated

$$S = \Delta V / \Delta T \tag{2}$$

here ΔV is the electric potential difference measured across the TE material, and ΔT is the temperature difference to which the material is exposed.

As for the state-of-the-art materials, bismuth telluride-based composites (BiTe) are one of the most used in TE applications, achieving ZT values of 1.86 at 320 K for p-type BiSbTe [16] and 1.15 at 400 K for n-type BiTeSe [17]. Besides inorganic materials, conjugated polymers have been also applied as TE materials, which may be advantageous due to their tunable electrical conductivity, mechanical flexibility, and low-cost processing methods [18], [19], [20]. Poly(3,4-ethylenedioxythiophene) polystyrene sulfonate (PEDOT:PSS) composites, in particular, have significant ZT values, reaching 0.42 at room temperature [21]. Composites of carbon nanotubes/conductive polymers have also been widely studied. For instance, SWCNT/PEDOT:PSS achieved a ZT of 0.4 at room temperature [22]. Another hotspot in thermoelectricity is the polymer composites combined with inorganic semiconductors, which have aroused intense interest from the scientific community. An example is bismuth telluride (Bi_2Te_3) with PEDOT, whose ZT was 0.58 with Seebeck coefficient of $\sim$180 μV/K at room temperature [23].

A measurement system used to accurately determine the Seebeck coefficient must be able to apply and maintain a stable temperature difference to the sample, while measuring the Seebeck voltage generated across the sample. It is essential to thermally isolate the sample holder, to avoid the influence of heat exchange with the external environment (heat loss). Indeed, a few systems have been proposed to determine the Seebeck coefficient. For instance, Zhang and collaborators described a system capable of measuring the Seebeck coefficient from -100 °C to 150 °C, specifically for inorganic bulk materials [24]. Similarly, Mishra et al. developed a system that can measure the Seebeck coefficient of inorganic bulk materials at temperatures up to 900 K [25]. More recently, Martin and Nolas [26], Fu et al. [27], and Narjis et al. [28] proposed a measurement apparatus to determine the Seebeck coefficient and electrical conductivity in bulk materials simultaneously. Also, Mulla et al. [29] introduced an easy-to-fabricate, cost-effective measurement system to evaluate the Seebeck coefficient. However, the system is designed for bulk TE materials, making it unsuitable for studying thin-film materials. Specifically, Mulla's system supports measurements up to 120 °C using basic thermocouples, which limits the accuracy of temperature measurement. Additionally, the absence of a chamber vacuum led to temperature stabilization issues [29]. Therefore, none of these proposals are tailored to accommodate thin-film-based TE technologies, such as π-conjugated TE devices. Furthermore, none provide the precise temperature control required for high-resolution measurements, which makes our apparatus uniquely suited for such applications. A table comparing the lab-made setups mentioned above for measuring Seebeck coefficient is provided in the Supplemental Material (Table S1). It is true that commercially available measuring systems exist for characterizing TE materials, such as ZEM-3 from ULVAC Company among many others. However, their high-cost makes them inaccessible to many scientists and research groups around the globe, making it essential to develop low-cost, easy-to-setup TE measuring systems.

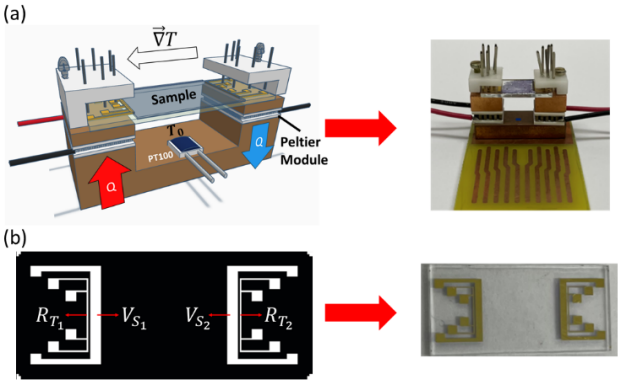

Fig. 1. (a) Scheme of the Seebeck coefficient measurement system, as well as the actual manufactured system. (b) Layout of the Seebeck coefficient measurement device, along with the manufactured device.

Here, we therefore focus on developing a low-cost, lab-made, and high-resolution system designed specifically to measure the Seebeck coefficient and electrical conductivity in thin-films technologies given their importance in the current development of TE devices. The system consists in a structure responsible for applying the temperature difference to the sample and a device structure capable of measuring the Seebeck voltage and temperature difference through the device itself. Furthermore, without the application of a temperature difference, the system allows the determination of the material's electrical conductivity of the material (through IV measurements) allowing the calculation of the PF (PF $= S^2\sigma$). The entire setup was built at a cost of US$ 300.00 and was designed to make the TE field accessible to everyone, especially those with limited scientific budgets.

II. Materials and Methods

A. Simulation and Development of the Measuring System

The ratio between the voltage generated and the temperature gradient to which a material is exposed is known as the Seebeck coefficient. A measurement system to determine the Seebeck coefficient must, therefore, allow for a temperature difference to be established between the two ends of a material. This can be accurately achieved by using two Peltier modules connected in series with reverse bias: when the modules are powered the temperature at one border of the sample increases while it decreases at the other border. In the system reported here, the Peltier modules are mounted on a copper block, as illustrated in Fig. 1(a), and are powered by a voltage source that controls the temperature difference applied to the sample. We have used a commercially available Peltier cooler module from Adaptive[1], model ET-017-08-15.

A spin-coated sample was used as proof of concept, with simultaneous measurements of the Seebeck voltage generated and the applied temperature difference. The material was deposited on a test device with two sets of electrodes

[1]Registered trademark.

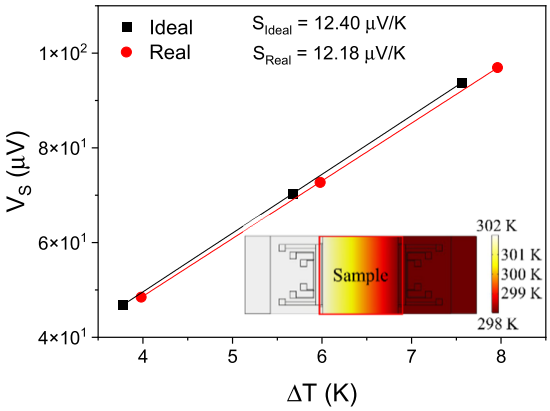

Fig. 2. Simulated Seebeck voltage as a function of the temperature difference, by the linear fitting the Seebeck coefficient of the sample was obtained. The simulated measurement device is shown in the inset.

(Vs_1 and Vs_2 in Fig. 1(b)), through which the voltage difference was measured between each end of the sample. The temperature difference was monitored through two gold strips in a 4-wire configuration (T_1 and T_2 sets as shown in Fig. 1(b)), which are used as thermometers. To establish the electrical connection between the thermometers and the voltage probe tips, pins arranged on a 3D-plastic plate are used, creating electrical contacts through pressure. Fig. 1 shows the scheme and layout of the measurement device, in addition to a photography of the actual item. Construction details, the design file of the 3D-plastic plate and the copper support illustrated in Fig. 1(a) can be found in Fig. S1. The design file is available in the Supplemental Material, as "3D-plastic plate.dwg."

The temperature difference across the sample should ideally be measured at the exact same location of the measurement of the Seebeck voltage. However, this is not practical unless extra insulating layers are added; otherwise, one would overlap two distinct electrodes. Therefore, the temperature-measuring electrodes and the voltage-measuring electrodes are patterned slightly displaced from one another. Since such displacement may introduce errors, we simulated the electrode pattern using the TE module in COMSOL software to verify the difference between stacked and non-stacked electrodes. The device was simulated considering gold electrodes on a Pyrex substrate and a thin film of PEDOT:PSS (200 nm) as the TE layer. All physical parameters used in the simulation are presented in Table S2 in the Supplemental Material. The Seebeck coefficient was calculated for two scenarios: 1) assuming the ideal case of temperature and voltage being measured at precisely the same location (ideal) and 2) considering slightly different locations for the gold strips and voltage electrodes (real). Fig. 2 shows the simulated measurement device along with the Seebeck voltage for several temperature differences applied to the sample. Upon analyzing the simulation results, one concludes that the location where the temperature is measured does not interfere significantly with the determination of the Seebeck coefficient [as can be seen in Fig. 2(b)]. The difference is less than 2%. Also, the Seebeck coefficient values obtained through $V_S \times \Delta T$ slope are similar to the value inferred from the PEDOT:PSS properties, 12.40 μV/K (Table S1). Also, simulations were performed considering different thickness of PEDOT:PSS thin film, which demonstrated that the thickness does not affect significantly the Seebeck coefficient obtained (Fig. S2).

Device's gold patterns to measure the Seebeck coefficient were produced by photolithography, with gold strips and electrodes deposited on glass substrates using the shadow masks presented in Fig. 1(b). Two electrodes (R_{T_1} and R_{T_2}) with a 4-wire configuration allow one to measure the temperature difference applied to the material through the change in their electrical resistances. In addition, the device has two metallic contacts (V_{S_1} and V_{S_2}), which are used to obtain the Seebeck voltage generated. It is required that the substrate presents insulating properties, since the use of a (semi)conductive material, even spaced by an additional insulating layer, can interfere in the measured Seebeck voltage due to parasitic field-effects. Because the Seebeck coefficient is temperature-dependent, fluctuations of the room temperature and potential electromagnetic interference were minimized by measuring the system under a metal vacuum chamber (Faraday cage-like) and within a controlled/stable laboratory condition. We used a lab-made vacuum chamber and a thermal bath Nova Ética model 521.3 DE to control base temperature (T_0). The base temperature T_0 of the system was determined using a PT100 resistance on a Cu block under the Peltier cooler modules [as discussed in Fig. 1(a)]. By controlling T_0, the TE properties of the sample can be characterized over a wide range of temperatures, from −20 °C to 100 °C. The Seebeck voltage and the temperature difference were measured with a nanovoltmeter model Keithley 2182A and sourcemeter model Keithley 2401, respectively. The cost of these devices may hamper the implementation of this measuring system, but low-cost resistance meters [30], [31], [32] and low-cost nanovoltmeters [33] can be found.

B. Manufacturing of the Seebeck Coefficient Device

The measuring device was fabricated using glass plates as substrate with dimensions of 50 × 70 mm^2. To obtain the gold pattern strips, the following steps were taken. First, a soft bake at 118 °C during 10 min was performed to dry the substrate surface. In order to improve the photoresist adherence, a hexamethyldisilazane (HDMS) thin film was deposited via spin-coating, 2500 r/min for 30 s, and baked using a hot plate at 118 °C during 5 min. The photoresist AZ 5214 E (MicroChemicals), used in the positive tone, was deposited using a spinner at 2500 r/min for 30 s, then the photoresist film was heated during 5 min at 118 °C. The photoresist was exposed to a UV light at 300 nm with 10 mW/cm^2 during 15 s. The pattern was obtained removing the exposed photoresist using a MIF312 solution (1:1) with water for 10 s at room temperature. Lastly, a 100 nm thick gold strip was deposited via physical vapor deposition (PVD) and the pattern was obtained removing the photoresist with acetone solution. For improving adhesion, a 20 nm thick Cr was deposited before the gold film deposition.

C. Measurements of the Seebeck Coefficient

To obtain the temperature difference across the TE device, a calibration was performed for the gold strips

as thermometers. The temperature was related to the electrical resistance of the thermometers using (3) [13], [19], [34]

$$R(T) = R_0 + \frac{dR}{dT}(T - T_0) \tag{3}$$

where T_0 is the initial temperature, R_0 is the initial resistance, dR/dT is the temperature-dependent resistance factor, and T is the final temperature. By measuring the resistance of the thermometer at different temperatures, dR/dT can be obtained through the tangent of the $R_0 \times T$ curve. It is worth mentioning that the Joule self-heating on electrical resistance can generate incorrect value for R_0. To avoid such a measurement error, R_0 was obtained by the linear fitting of the IV curve.

The Seebeck coefficient of the material ($S = V_S/\Delta T$) was determined from the slope of the $V_S \times \Delta T$ curve. The temperature gradient across the sample was varied altering the voltage on the Peltier modules. For each voltage applied, the temperature difference and the Seebeck voltage were measured simultaneously to determine the Seebeck coefficient. Offset voltage values can be generated by temperature difference at the connections between different materials. To mitigate these effects, the Seebeck coefficient was obtained by fitting the $V_S \times \Delta T$ curve. Also, the influence of the small temperature oscillations is reduced, thereby improving the precision of the measurement system.

For the error calculation, the resolution of the different pieces of the measuring systems were considered. Moreover, a statistical analysis was performed on the number of measurements, and error propagation was carried out as described in the next section.

D. Uncertainty in the Measurements and Error Calculation

In order to improve the reliability of the results, several measurements were performed, allowing to obtain an average value. Moreover, the uncertainty of the results was verified considering the standard deviation. Therefore, for each temperature at the border of the material, 5 measurements were taken, while for each Seebeck voltage generated by the sample, 10 measurements were performed. The standard deviation was calculated using the following formula:

$$\mu = \sqrt{\frac{1}{n-1}\sum_{i=1}^{n}(x_i - \bar{x})^2} \tag{4}$$

where n is the total number of measurements performed, x_i is the value of the i-n measurement and $\bar{x}$ is the average of all measurements. Since the result depends on several measured variables, the total uncertainty can be estimated through error propagation. If the value F is a function of the variables x, y, z, the total uncertainty (u_F) is given by

$$u_F = \sqrt{\left(\frac{\partial F}{\partial x}u_x\right)^2 + \left(\frac{\partial F}{\partial y}u_y\right)^2 + \left(\frac{\partial F}{\partial Z}u_z\right)^2} \tag{5}$$

where $(\partial F/\partial x)$, $(\partial F/\partial y)$, $(\partial F/\partial z)$ are the partial derivatives of F with respect to the variables x, y, z and u_x, u_y, u_z are the uncertainties associated with each independent variable.

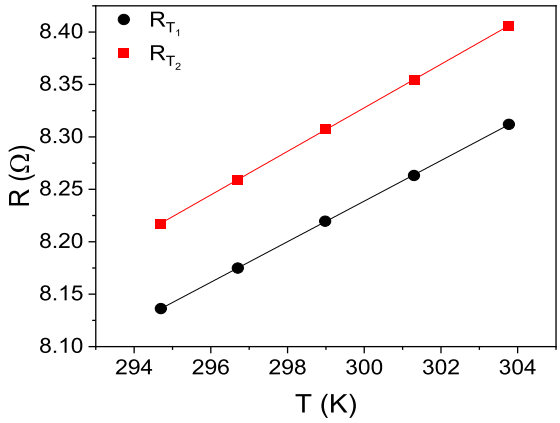

Fig. 3. Resistance of the gold contacts of the four-point system R_{T_1} and R_{T_2} as a function of the temperature. The uncertainty intervals are narrower than the data points.

E. Measurements of Electrical Conductivity and the Calculation of the PF

The resistance of the sample was measured using the same experimental setup, but without applying a temperature gradient (Peltier modules turned off). From the sample resistance, its electrical conductivity was calculated using (6) [13], [19], [34]

$$\sigma = \frac{L}{R \cdot A} \tag{6}$$

where L is the length of the sample, R is the resistance of the sample, and A is the cross-sectional area through which the charge carriers flow. To determine the cross-sectional area of the sample, a Veeco Dektak 150 Profilometer was used. The PF of the material studied could then be calculated using ($\mathrm{PF} = S^2.\sigma$) [8], [9], [10], [13].

III. Results and Discussion

A. Calibration of the Experimental Setup

The measurement system was characterized by calibrating the two gold strips in Fig. 1(b). This was performed by measuring the electrical resistances of the two thermometers (R_{T_1} and R_{T_2}) at five temperatures (T_0 = 294.70 ± 0.05 K; 296.70 ± 0.05 K; 298.90 ± 0.05 K; 301.30 ± 0.05 K; 303.80 ± 0.05 K), which were set by the thermal bath. The electrical resistances were measured by a sourcemeter Keithley 2401 in 4-wire configuration. The temperature coefficient of resistance (TCR) was obtained from the slope of the $R \times T$ curve in which the electrical resistances were associated with the temperatures of the thermal bath. The exact temperature at each end of the device was measured with calibrated gold thermometers. Different devices were measured, consistently exhibiting linear behavior, thereby enabling their use as thermometers (Fig. S3), with uncertainty lower than 0.02%. Fig. 3 shows the electrical resistance as a function of the temperature for each thermometer and the linear fit.

Fig. 4 shows the temperature at the borders of the device and the temperature difference as a function of the voltage applied to the Peltier modules. The measurements were carried out with a base temperature (T_0) at 298.00 ± 0.05 K and

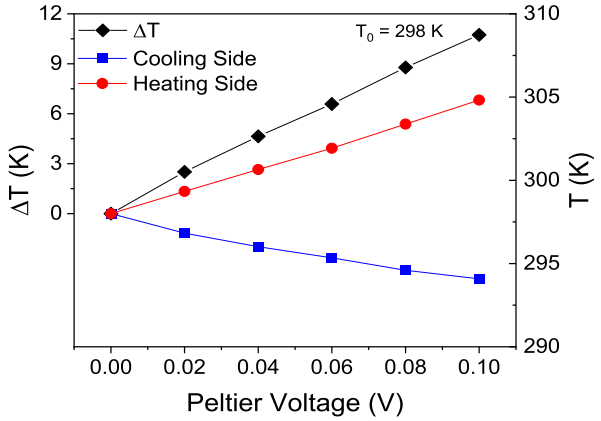

Fig. 4. Temperature of the hot and cold side as a function of the voltage applied to the Peltier cells. Base temperature at 298 K. The error bars are smaller than the data points.

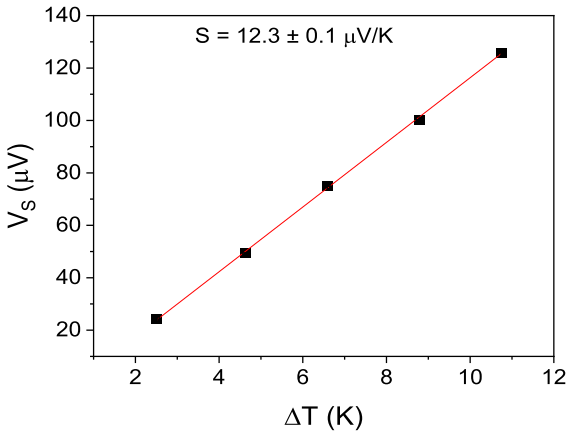

Fig. 5. Seebeck voltage of PEDOT:PSS as a function of the temperature difference. The uncertainty intervals are narrower than the data points.

at the thermal stationary state, which was established around 15 min after turning on the Peltier modules. The temperature at the cold side decreased, reaching 294.10 ± 0.05 K for 0.1 V, while the hot side reached 304.80 ± 0.05 K. Thus, a temperature difference of 10.7 ± 0.1 K was obtained for 0.1 V. This temperature difference increases linearly with the voltage, facilitating the association of the voltage applied to the Peltier modules with the temperature difference on the sample.

B. Measurements of the Test Sample

The system was validated by measuring the Seebeck coefficient of a PEDOT:PSS thin film (Baytron PH1000, supplied by Heraeus). This film was spin-coated on the gold tracks (Vs_1 and Vs_2) shown in Fig. 1. For spin coating, 5 vol% of ethylene glycol (EG, Mallinckrodt) and 0.1 vol% of dodecylbenzene sulfonic acid (DBSA, Aldrich) were added to the PEDOT:PSS solution, resulting in a thin 115 nm thick film. The Seebeck voltage was measured for five temperature differences (ΔT = 2.5 ± 0.1 K; 4.6 ± 0.1 K; 6.6 ± 0.1 K; 8.8 ± 0.1 K; 10.7 ± 0.1 K), and the Seebeck coefficient (S) was calculated from the slope of the $V_S \times \Delta T$ curve. Fig. 5 shows the open-circuit Seebeck voltage generated by PEDOT:PSS thin film as a function of the temperature difference, leading to a Seebeck coefficient of 12.3 ± 0.1 μV/K. This value is consistent with the literature that used similar film thickness, where the PEDOT:PSS Seebeck coefficient ranges from 11 μV/K to 27 μV/K [21], [35], [36].

The resistance of the PEDOT:PSS film was obtained via IV curve (Fig. S4 in the Supplemental Material) and the electrical conductivity was calculated using (6). The electrical conductivity was 491.0 ± 0.1 S/cm, yielding a PF of 7.5±0.1 μW/K^{2}m, compatible with the literature values [21], [35], [36].

IV. Conclusion

This work was aimed at designing and constructing a low-cost measurement system capable to determine the Seebeck coefficient and electrical conductivity of thin films. The system developed permitted to apply a temperature difference at the ends of a sample while simultaneously measuring the Seebeck voltage generated. The Seebeck coefficient of the sample could then be determined. The measurement system was validated by measuring a PEDOT:PSS thin film, which was subjected to five temperature differences. The Seebeck coefficient of PEDOT:PPS film was 12.3 ± 0.1 μV/K, which agrees with the values reported in the literature. Using the resistance measurement and considering the sample dimensions the electrical conductivity was obtained, 491.0 ± 0.1 S/cm. Then, a PF of 7.5 ± 0.1 μW/K^{2}m was calculated, again as expected from the literature. Our results show the high resolution of the system, as evidenced by the obtained values of 0.1 μV/K for the Seebeck coefficient, 0.1 S/cm for electrical conductivity, and 0.1 μW/K^2 for the PF. The simplicity of the system and its low cost allow any lab to measure the Seebeck coefficient, particularly if low-cost nanovoltmeters are available.

Acknowledgment

This research used facilities of the Brazilian Nanotechnology National Laboratory (LNNano), part of the Brazilian Center for Research in Energy and Materials (CNPEM), a private nonprofit organization under the supervision of the Brazilian Ministry for Science, Technology, and Innovations (MCTI). The microfabrication staff is acknowledged for assistance during the experiments of the proposal number 20232235.

References

[1] J. He, K. Li, L. Jia, Y. Zhu, H. Zhang, and J. Linghu, "Advances in the applications of thermoelectric generators," *Appl. Thermal Eng.*, vol. 236, Jan. 2024, Art. no. 121813, doi: 10.1016/j.applthermaleng.2023.121813.

[2] N. Van Toan, T. T. K. Tuoi, N. Van Hieu, and T. Ono, "Thermoelectric generator with a high integration density for portable and wearable self-powered electronic devices," *Energy Convers. Manage.*, vol. 245, Oct. 2021, Art. no. 114571, doi: 10.1016/j.enconman.2021.114571.

[3] F. Suarez, A. Nozariasbmarz, D. Vashaee, and M. C. Öztürk, "Designing thermoelectric generators for self-powered wearable electronics," *Energy Environ. Sci.*, vol. 9, no. 6, pp. 2099–2113, 2016, doi: 10.1039/c6ee00456c.

[4] L.-Q. Liu, Z.-X. Wang, H.-Q. Zhang, and Y.-C. Xue, "Solar energy development in China—A review," *Renew. Sustain. Energy Rev.*, vol. 14, no. 1, pp. 301–311, Jan. 2010, doi: 10.1016/j.rser.2009.08.005.

[5] M. Londres. *Energia Solar: Fim Do Subsídio*. Accessed: Apr. 10, 2024. [Online]. Available: https://economia.uol.com.br/colunas/mariana-londres/2023/01/02/eletrica-subsidios-senado.htm

[6] U. R. Pagel, A. F. Campos, and J. Carolino. *Análise dos Principais Desafios ao Desenvolvimento das Energias Renováveis no Brasil*. Accessed: Apr. 10, 2024. [Online]. Available: https://engenhariaedesenvolvimentosustentavel.ufes.br/sites/engenhariaedesenvolvimentosustentavel.ufes.br/files/field/anexo/artigo_analise_dos_principais_desafios_2.pdf

[7] J. M. Cullen and J. M. Allwood, "Theoretical efficiency limits for energy conversion devices," *Energy*, vol. 35, no. 5, pp. 2059–2069, May 2010, doi: 10.1016/j.energy.2010.01.024.

[8] F. J. DiSalvo, "Thermoelectric cooling and power generation," *Science*, vol. 285, no. 5428, pp. 703–706, Jul. 1999, doi: 10.1126/science.285.5428.703.

[9] H. S. Kim, W. Liu, G. Chen, C.-W. Chu, and Z. Ren, "Relationship between thermoelectric figure of merit and energy conversion efficiency," *Proc. Nat. Acad. Sci. USA*, vol. 112, no. 27, pp. 8205–8210, Jul. 2015, doi: 10.1073/pnas.1510231112.

[10] B. Poudel et al., "High-thermoelectric performance of nanostructured bismuth antimony telluride bulk alloys," *Science*, vol. 320, no. 5876, pp. 634–638, May 2008, doi: 10.1126/science.1156446.

[11] J. Yang and T. Caillat, "Thermoelectric materials for space and automotive power generation," *MRS Bull.*, vol. 31, no. 3, pp. 224–229, Mar. 2006, doi: 10.1557/mrs2006.49.

[12] L. Catalan, P. Alegria, M. Araiz, and D. Astrain, "Field test of a geothermal thermoelectric generator without moving parts on the hot dry rock field of timanfaya national park," *Appl. Thermal Eng.*, vol. 222, Mar. 2023, Art. no. 119843, doi: 10.1016/j.applthermaleng.2022.119843.

[13] D. M. Rowe, *Thermoelectrics Handbook: Macro to Nano*, 2005.

[14] G. J. Snyder and E. S. Toberer, "Complex thermoelectric materials," *Nature Mater.*, vol. 7, no. 2, pp. 105–114, Feb. 2008, doi: 10.1038/nmat2090.

[15] Q. Zhang, Y. Sun, W. Xu, and D. Zhu, "Organic thermoelectric materials: Emerging green energy materials converting heat to electricity directly and efficiently," *Adv. Mater.*, vol. 26, no. 40, pp. 6829–6851, Mar. 2014, doi: 10.1002/adma.201305371.

[16] S. I. Kim et al., "Dense dislocation arrays embedded in grain boundaries for high-performance bulk thermoelectrics," *Science*, vol. 348, no. 6230, pp. 109–114, Apr. 2015, doi: 10.1126/science.aaa4166.

[17] S. Wang, H. Li, R. Lu, G. Zheng, and X. Tang, "Metal nanoparticle decorated n-type Bi_2Te_3-based materials with enhanced thermoelectric performances," *Nanotechnology*, vol. 24, no. 28, Jul. 2013, Art. no. 285702, doi: 10.1088/0957-4484/24/28/285702.

[18] S. R. Forrest, "The path to ubiquitous and low-cost organic electronic appliances on plastic," *Nature*, vol. 428, no. 6986, pp. 911–918, Apr. 2004, doi: 10.1038/nature02498.

[19] M. Culebras, C. Gómez, and A. Cantarero, "Review on polymers for thermoelectric applications," *Materials*, vol. 7, no. 9, pp. 6701–6732, Sep. 2014, doi: 10.3390/ma7096701.

[20] S. Masoumi, S. O'Shaughnessy, and A. Pakdel, "Organic-based flexible thermoelectric generators: From materials to devices," *Nano Energy*, vol. 92, Feb. 2022, Art. no. 106774, doi: 10.1016/j.nanoen.2021.106774.

[21] G.-H. Kim, L. Shao, K. Zhang, and K. P. Pipe, "Engineered doping of organic semiconductors for enhanced thermoelectric efficiency," *Nature Mater.*, vol. 12, no. 8, pp. 719–723, Aug. 2013, doi: 10.1038/nmat3635.

[22] S. Liu, H. Li, and C. He, "Simultaneous enhancement of electrical conductivity and Seebeck coefficient in organic thermoelectric SWNT/PEDOT:PSS nanocomposites," *Carbon*, vol. 149, pp. 25–32, Aug. 2019, doi: 10.1016/j.carbon.2019.04.007.

[23] L. Wang et al., "Exceptional thermoelectric properties of flexible organic–inorganic hybrids with monodispersed and periodic nanophase," *Nature Commun.*, vol. 9, no. 1, p. 3817, Sep. 2018, doi: 10.1038/s41467-018-06251-9.

[24] L. Zhang, X. Chen, J. Sun, H. Cai, H. Li, and D. Cui, "Development of Seebeck coefficient measurement system with wide range of temperatures for inorganic material measurement," in *Proc. IEEE 10th Int. Conf. Intell. Sensors, Sensor Netw. Inf. Process. (ISSNIP)*, Apr. 2015, pp. 1–4, doi: 10.1109/ISSNIP.2015.7106940.

[25] A. Mishra, S. Bhattacharjee, and S. Anwar, "Simple apparatus to measure Seebeck coefficient up to 900K," *Measurement*, vol. 68, pp. 295–301, May 2015, doi: 10.1016/j.measurement.2015.03.005.

[26] J. Martin and G. S. Nolas, "Apparatus for the measurement of electrical resistivity, Seebeck coefficient, and thermal conductivity of thermoelectric materials between 300 K and 12 K," *Rev. Scientific Instrum.*, vol. 87, no. 1, Jan. 2016, Art. no. 015105, doi: 10.1063/1.4939555.

[27] Q. Fu, Y. Xiong, W. Zhang, and D. Xu, "A setup for measuring the Seebeck coefficient and the electrical resistivity of bulk thermoelectric materials," *Rev. Sci. Instrum.*, vol. 88, no. 9, Sep. 2017, Art. no. 095111, doi: 10.1063/1.4990634.

[28] A. Narjis, M. Elyaagoubi, A. Outzourhit, and L. Nkhaili, "Design of a simple apparatus for the measurement of the Seebeck coefficient," *Measurement*, vol. 133, pp. 433–438, Feb. 2019, doi: 10.1016/j.measurement.2018.10.038.

[29] R. Mulla, K. Glover, and C. W. Dunnill, "An easily constructed and inexpensive tool to evaluate the Seebeck coefficient," *IEEE Trans. Instrum. Meas.*, vol. 70, pp. 1–7, 2021, doi: 10.1109/TIM.2020.3021512.

[30] R. Mitchell. *Build Your Own Low-Resistance Meter*. Accessed: May 19, 2024. [Online]. Available: https://www.allaboutcircuits.com/projects/build-your-own-low-resistance-meter/

[31] ADI Engineer Zone. *Measure Very Small Resistances by Building Your Own Milliohm-meter*. Accessed: May 19, 2024. [Online]. Available: https://ez.analog.com/adieducation/university-program/b/blogs/posts/measure-very-small-resistances-by-building-your-own-milliohm-meter

[32] Bob Nuckolls. *Practical Low Resistance Measurements*. Accessed: May 19, 2024. [Online]. Available: http://www.aeroelectric.com/articles/LowOhmsAdapter_3.pdf

[33] G. Cannatà, G. Scandurra, and C. Ciofi. (2012). *Nanovoltmeter Amplifier for Low Level Voltage Measurements*. Accessed: May 19, 2024. [Online]. Available: file:///D:/Nanovoltmeter_amplifier_for_low_level_voltage_measurements.pdf

[34] S. Peng et al., "A review on organic polymer-based thermoelectric materials," *J. Polym. Environ.*, vol. 25, no. 4, pp. 1208–1218, Dec. 2017, doi: 10.1007/s10924-016-0895-z.

[35] Z. Fan, P. Li, D. Du, and J. Ouyang, "Significantly enhanced thermoelectric properties of PEDOT:PSS films through sequential post-treatments with common acids and bases," *Adv. Energy Mater.*, vol. 7, no. 8, Apr. 2017, Art. no. 1602116, doi: 10.1002/aenm.201602116.

[36] J. Atoyo, M. R. Burton, J. McGettrick, and M. J. Carnie, "Enhanced electrical conductivity and Seebeck coefficient in PEDOT:PSS via a two-step ionic liquid and $NaBH_4$ treatment for organic thermoelectrics," *Polymers*, vol. 12, no. 3, p. 559, Mar. 2020, doi: 10.3390/polym12030559.